Supplementary Information

Anchoring Ruthenium Nanoclusters by an Electron-Donating Fullerene Carbon Matrix for High-Performance Hydrogen Evolution

*Ying Wang[a], Yongqiang Feng[*a], Jun Zhang[a], Qunzhi Ma[a], Jiayi Li[a], Wei Liu[a], Wenyu Wang[a], Yirong Qi[a], Qingqing Liu[a], Xu Li[a], Xiaojie Ma[a]*

[a] *School of Materials Science and Engineering, Shaanxi University of Science and Technology, Xi'an 710021, China*

Corresponding authors: fengyq@sust.edu.cn

Content

Experimental Sections

1. General material

All chemical reagents were used as received without any further purification. Ruthenium trichloride ($RuCl_3$, 99%), potassium hydroxide (KOH, ≧ 90%), Nafion solution (5 wt.%), Pt/C (20 wt.%), Pluronic P123 tri-block copolymer (PEG-PPG-PEG, molecular mass = 5800), 1-chloronaphthalene, hydrofluoric acid (HF, 98%), tetraethyl orthosilicate (TEOS, $C_8H_{20}OSi$, 98%), Sodium borohydride ($NaBH_4$, 99%), isopropyl alcohol (IPA, $(CH_3)_2CHOH$, ≧ 99.7%) and hydrochloric acid (HCl, 36~38%), ethanol (EtOH, CH_3CH_2OH, 99.7%) were purchased from Sinopharm Chemical Reagent Co., Ltd. Fullerene (C_{60}, 99.9%) was received from Beijing Funakang Biotechnology Co., Ltd. The hydrophilic carbon paper (CP) was purchased from CeTech Co., Ltd. The anion exchange membrane (3PK-130) was obtained from Wuhan Gaoshi Ruilian Technology Co., Ltd. Deionized water (DI, 18.25 MΩ/cm) was produced from the ultra-pure purification system (ULUPURE, UPDR-I-10T).

2. Synthesis of defective fullerene carbon fragment (FCF)

The mesoporous template of SBA-15 was synthesized according to the literature.[1] Briefly, 2 g of P123 was first dissoved in 58 mL of 2 M HCl, TEOS was then slowly added and heated at 40 ºC for 12 h. The mixture was then transferred into a Teflon-lined autoclave capped with a stainless steel vessel. After heating at 130 ℃ for 48 h, the precipitate was collected, washed with DI water and dried at 100 ºC for 6 h followed by calcination at 540 ºC. For the preparation of MFC_{60-x}, a modified approach was employed.[1] First, a saturated solution of fullerene C_{60} was prepared by dissolving 50

mg of C_{60} in 5 mL of 1-chloronaphthalene. The SBA-15 mesoporous material was then impregnated with this solution for 48 h, allowing C_{60} molecules to assemble within the pores. The resulting solid product, C_{60}/SBA-15, was annealed at 900 °C for 5 h under an argon atmosphere to enhance the interaction between C_{60} and the SBA-15 matrix. Finally, the template was removed by etching with hydrofluoric acid (HF), and the final sample was designated as FCF.

3. Synthesis of Ru/FCF-600, Ru/FCF-500 and Ru/FCF-700.

The Ru/FCF-600 HER electrocatalyst was synthesized via a $NaBH_4$ reduction combined with solid-phase sintering method, with the detailed procedure as follows: First, 43.5 mg of FCF was dispersed in a mixed solvent of ethanol (EtOH) and deionized water (DI water) (v/v = 1:2). Subsequently, 13 mg of $RuCl_3$ was impregnated into the above solution and vigorously stirred at 25 °C for 1 h to ensure thorough mixing. Next, a freshly prepared $NaBH_4$ solution (1 mg mL^{-1}) was slowly added dropwise over 2 h under continuous stirring at room temperature. After complete addition, the reaction was allowed to proceed for an additional 2 h to ensure complete reduction. The resulting product was then filtered and washed multiple times with DI water and ethanol to remove impurities. The obtained solid was vacuum-dried at 60 °C for 12 h to yield the Ru/FCF precursor. The black powder obtained was placed in a corundum porcelain boat under the protection of Ar mixture in a tubular furnace, heated from room temperature to 600 °C at a heating rate of 5 °C min^{-1} , and kept for 2 h. After cooling to room temperature, the black powder was collected and ground to obtain the target product Ru/FCF-600 electrocatalyst. For comparison, under identical experimental conditions,

Ru/FCF-500 and Ru/FCF-700 electrocatalysts were synthesized by adjusting the calcination temperature to 500 °C and 700 °C, respectively, to investigate the influence of temperature on the catalytic performance.

4. Materials Characterization.

The X-ray diffraction (XRD) was tested using Cu Kα radiation (λ = 1.5406 Å) on a Rigaku D/max-2200PC diffractometer (Japan). The topography and structure of the sample were analyzed using a scanning electron microscope (SEM, S4800). Raman spectrum was recorded on a Renishaw-invia instrument. The transmission electron microscopy (TEM) was carried out on a Themis Z/ORION704M scanning/transmission electron microscope manipulated at 300 kV. X-ray photoelectron spectroscopy (XPS) was obtained on a Thermo Kalpha X-ray photoelectron spectrometer with Al Kα as the source gun. The electrochemical performance test was carried out on the CHI660E workstation (Shanghai Chenhua).

5. Electrochemical measurement.

The electrocatalytic performance was carried out on a CHI660E electrochemical workstation using a three-electrode system in 1 M KOH with glassy carbon electrode (GCE, Φ = 3 mm), graphitic rod and Hg/HgO as the working, counter and reference electrode, respectively. Before all tests, the Hg/HgO reference electrode was calibrated against the reversible hydrogen potential (RHE) in H_2-saturated 1 M KOH with Pt plate as the working electrode and Pt wire as the counter electrode. Thus, the potential can be obtained by the equation of E(RHE) = E(Hg/HgO) + 0.926 (Figure S9). To prepare the working electrode, 5 mg of catalyst was sonicated in 150 μL of IPA containing 8

μL of Nafion solution to form a homogeneous ink. Then, 2.4 μL of the suspension is loaded onto the polished GCE at a loading of 1.076 mg cm^{-2}. The linear scanning voltammetry (LSV) curve was recorded in a N_2-saturated 1 M KOH with a scan rate of 3 mV s^{-1}. Tafel slope was obtained by plotting the LSV curve using the equation of $\eta = a + b \log j$, where η refers to the overpotential, b is the Tafel slope and a denotes the intercept. The electrochemical impedance spectroscopy (EIS) were performed under open circuit potentials for all materials and the frequency range from 0.1 Hz to 100 kHz with an amplitude of 5 mV were used to carry out the experiment. For the specific double-layer capacitor (C_{dl}) data, cyclic voltammetry (CV) curves were recorded in the non-Faradic region with scanning rate of 2, 4, 6, 8, 10 and 12 mV s^{-1}, and the C_{dl} (mA cm^{-2}) can be obtained by plotting the current difference (Δj) against the scanning rate. The electrochemical active surface area (ECSA) was estimated by the following equation of $ECSA=Cdl / C_s \times S$, where Cs (μF cm^{-2}) represents the specific capacitance on the electrode surface and S (cm^2) is the actual area of the working electrode. Generally, C_s is in the range of 20-60 μF cm^{-2}, herein the averaged Cs value of 40 μF cm^{-2} was used according the literature.

The Faradic efficiency of gas evolution was carried out using the water drainage method:

$$\eta_F = \frac{N_F}{N_T} = \frac{mnF}{It}$$

Where N_F is the actual charge consumed, N_T is the total charge flowing through the external circuit, m is the number of moles of hydrogen, n is the electron transferred by the reaction, F is Faraday's constant 96485 C mol^{-1}, and I and t are the current and

reaction time, respectively.

Anion exchange membrane water electrolysis (AEMWE) measurement：

Prior to the fabrication of the anion-exchange membrane water electrolyzer (AEMWE) system, the anion exchange membrane (AEM) was pretreated by soaking in 1.0 M KOH solution for 24 hours. The catalyst slurries prepared with Ru/FCF-600 and IrO_2 were used as the active materials for the cathode and anode, respectively. Employing the catalyst-coated substrate method, 3 mg of the cathode catalyst and 3 mg of the anode catalyst were separately deposited on carbon cloth with a gas diffusion layer (GDL), each with an area of 1×1 cm^2. Subsequently, the AEMWE system was filled with 1.0 M KOH electrolyte, and the flow rate was controlled at 40 mL/min using a peristaltic pump. Thereafter, the performance of the AEMWE was evaluated using a Koster electrochemical workstation (CS310M) equipped with an electrocatalytic cell. The long-term stability of the device was tested via chronopotentiometry.

Calculation of the turnover frequency (TOF):

The turnover of frequency (TOF) was evaluated by CO-stripping measurement. Firstly, the prepared catalysts were tested in the N_2-saturated 1.0 M KOH solution, and CV curves from 0.05 to 1.00 V vs. RHE were measured at a scan rate of 10 mV s^{-1}. Secondly, a reduction potential (0.05 V vs. RHE) was applied to the working electrode while passing CO for 15 min, followed by N_2 for 15 min to drive the escape of excess CO out of the electrolyte. Then, re-running the CV test as described above, a distinct oxidation peak of CO can be observed at 0.6-0.8 V vs. RHE. Ultimately, the number of exposed active sites in the catalyst is determined by integrating the area of this oxidation

peak.

The TOF (s^{-1}) for HER can be obtained by the following equation:

$$TOF = \frac{I \times N_A}{2 \times F \times \Gamma}$$

Where I is the current (A) during the linear scaning process, N_A is Avogadro number, the factor 2 refers to two electrons required to produce one hydrogen molecule. F is the Faraday constant (96485 C mol^{-1}), and Γ is the number of exposed active sites.

Γ can be quantified by the CO stripping method and calculated from the following equation:

$$\Gamma = \frac{A_{under\ CO\ peak}}{2 \times e \times \nu}$$

where $A_{under\ CO\ peak}$ is the area of the CO oxidation peak, e is the charge of an electron, and ν is the scan rate through the CV scans.

Additional Figures and Tables

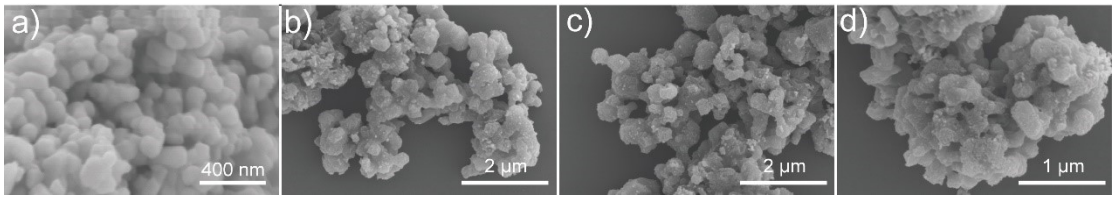

Figure S1. SEM image of a) C_{60}/SBA-15, b) FCF, c) Ru/FCF, d) Ru/FCF-600.

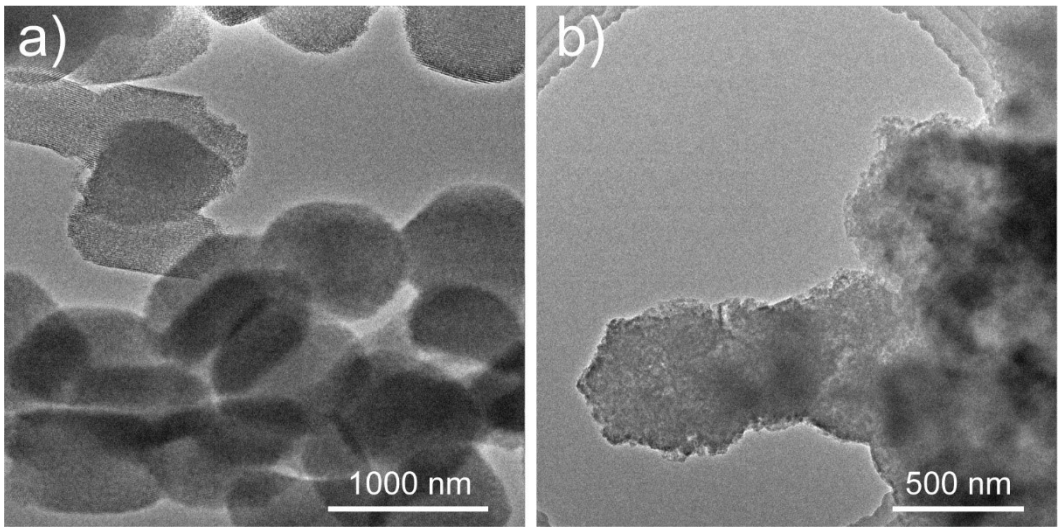

Figure S2. TEM images of a) SBA-15 and b) FCF.

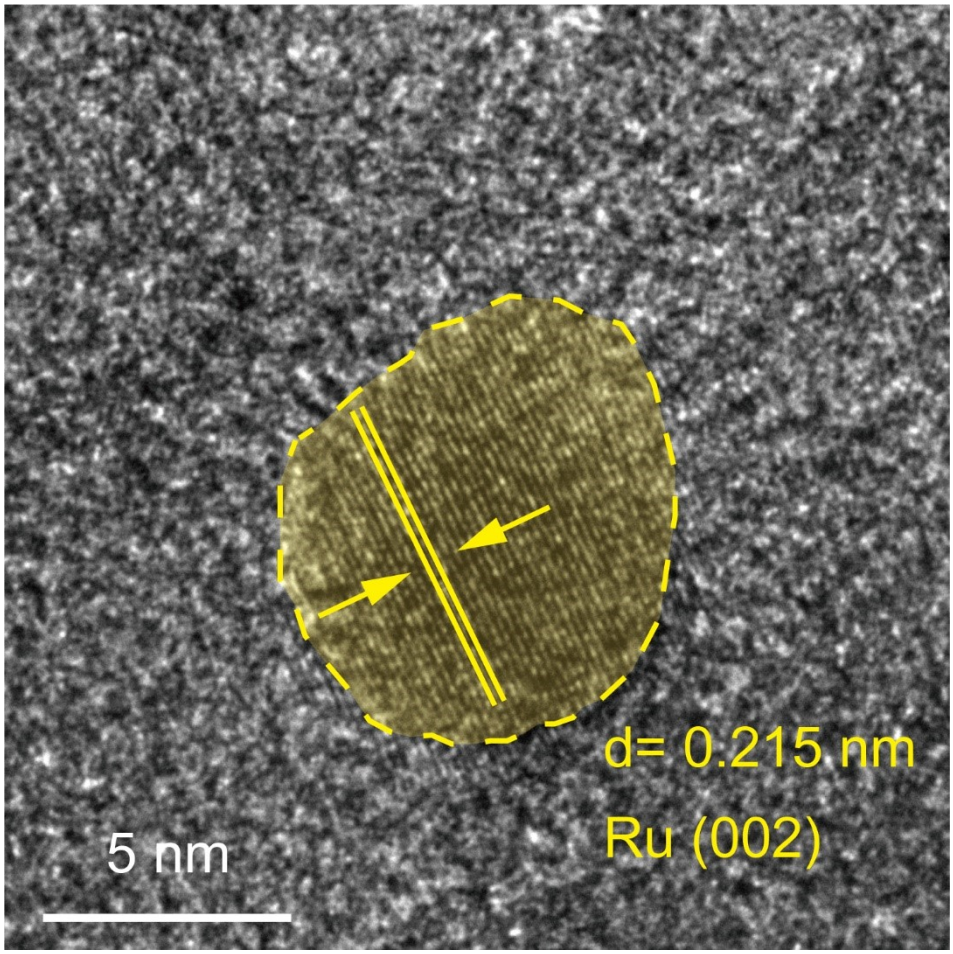

Figure S3. TEM images of the Ru/FCF-600.

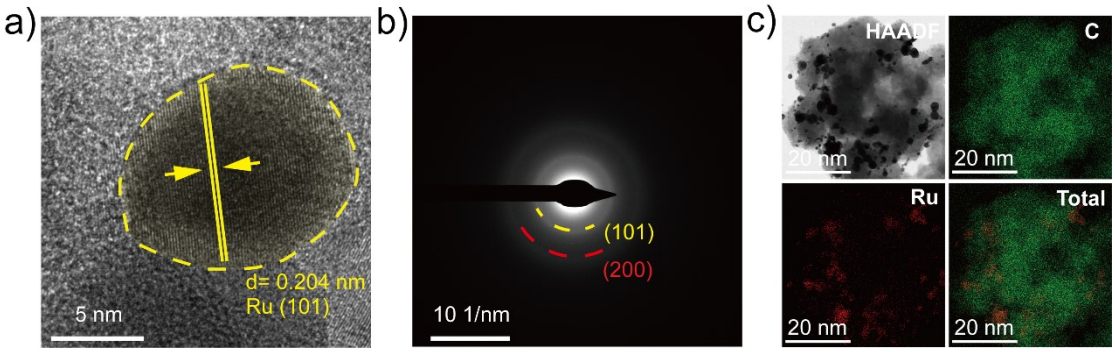

Figure S4. Structural and morphological characterization of Ru/FCF-500. a) HRTEM image, b) SAED pattern, c) Corresponding elemental mapping images of C (green) and Ru (red).

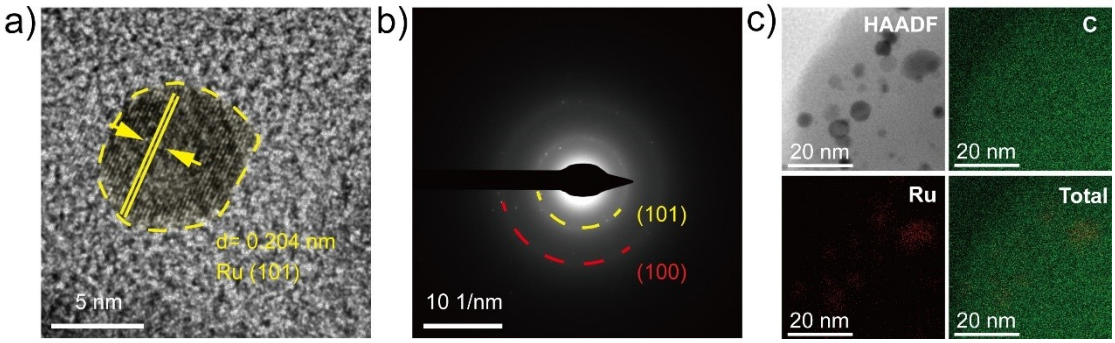

Figure S5. Structural and morphological characterization of Ru/FCF-700. a) HRTEM image, b) SAED pattern, c) Corresponding elemental mapping images of C (green) and Ru (red).

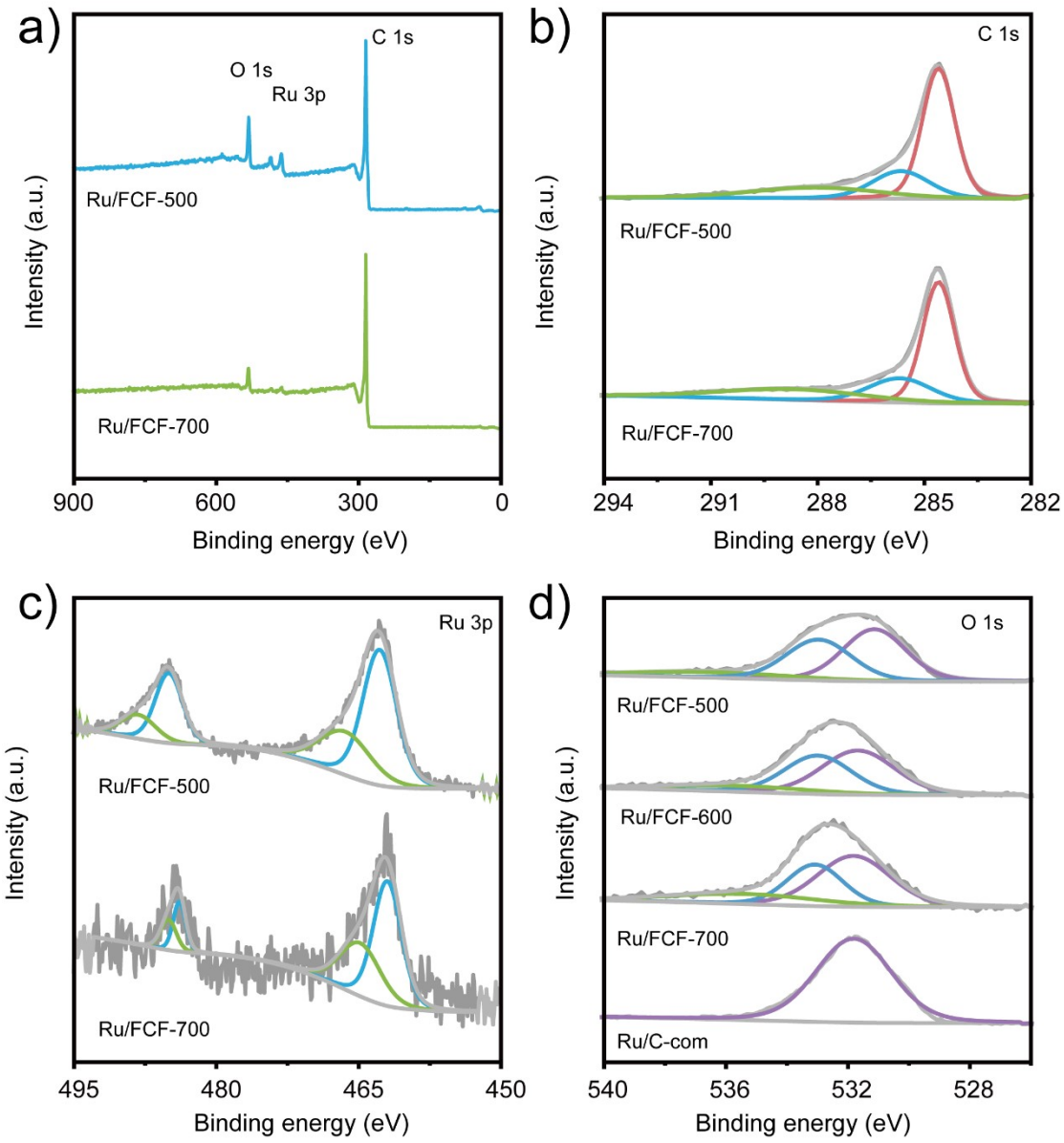

Figure S6. a) XPS survey spectra of Ru/FCF-500 and Ru/FCF-700. b) C 1s, c) Ru 3p spectra of Ru/FCF-500 and Ru/FCF-700. d) O 1s spectra of Ru/FCF-500, Ru/FCF-600, Ru/FCF-700, and commercial Ru/C.

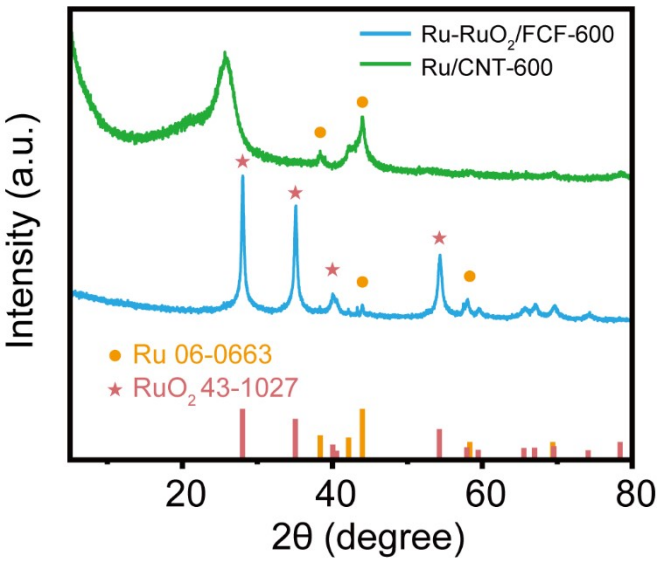

Figure S7. XRD patterns of Ru-RuO_2/FCF-600 and Ru/CNT-600.

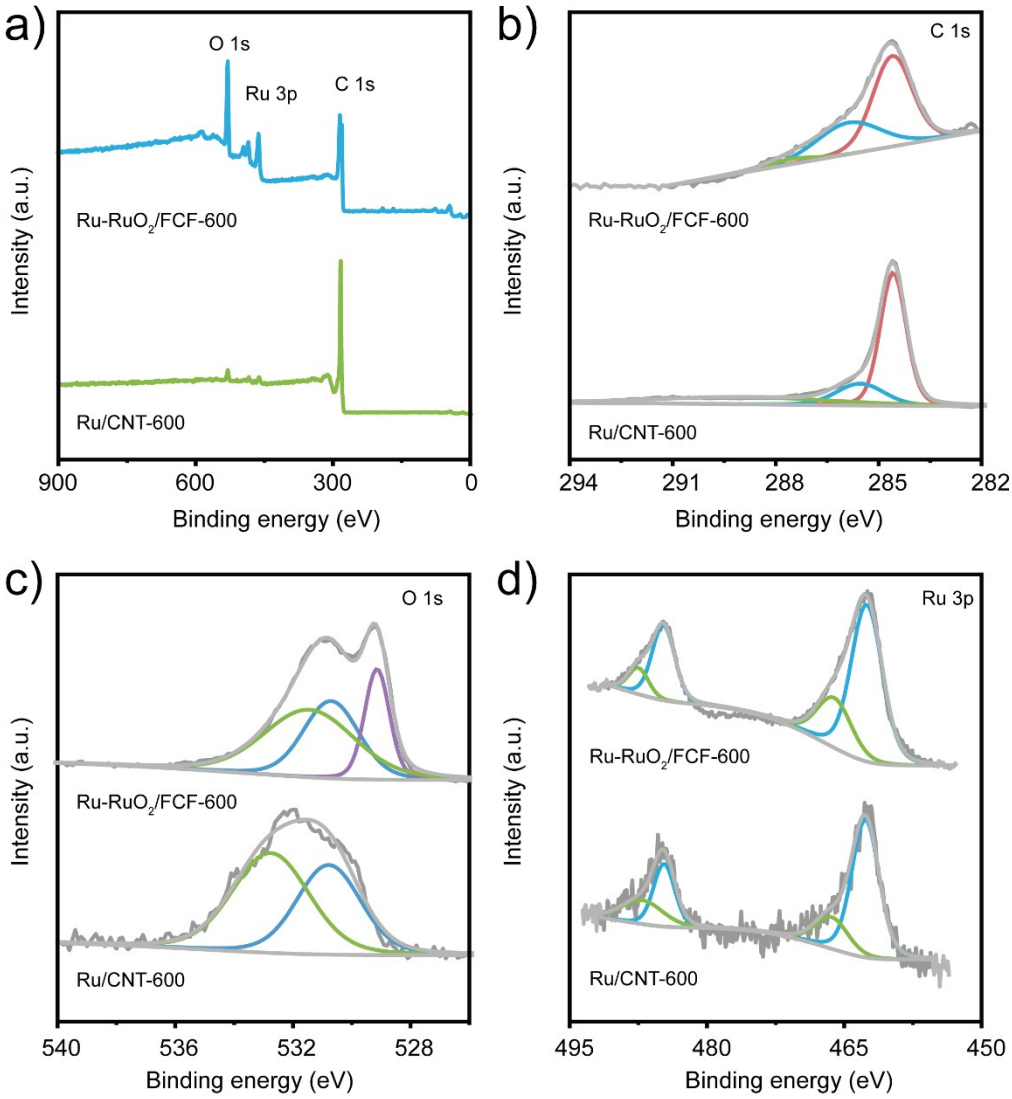

Figure S8. a) XPS survey spectra of Ru-RuO_2/FCF-600 and Ru/CNT-600. b) C 1s, c) Ru 3p spectra of Ru-RuO_2/FCF-600 and Ru/CNT-600. d) O 1s spectra of Ru-RuO_2/FCF-600 and Ru/CNT-600.

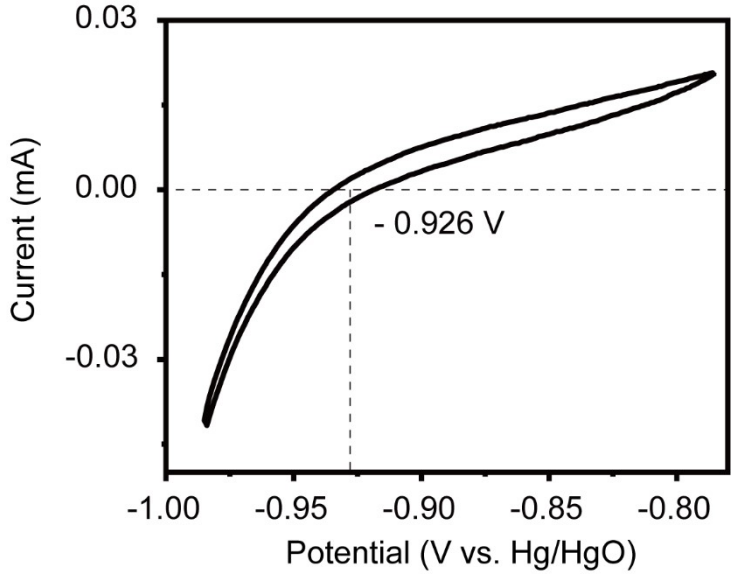

Figure S9. CV curve for calibration of Hg/HgO reference electrode in 1 M KOH.

Prior to all measurements, the reference electrode (Hg/HgO in alkaline medium) was calibrated against a reversible hydrogen electrode (RHE) in H_2-saturated electrolyte using a standard three-electrode system, with a Pt plate as the working electrode and a Pt wire as the counter electrode. The measured potentials were then converted to the RHE scale according to the following equation:

$$E(RHE) = E(Hg/HgO) + 0.926(1\ M\ KOH)$$

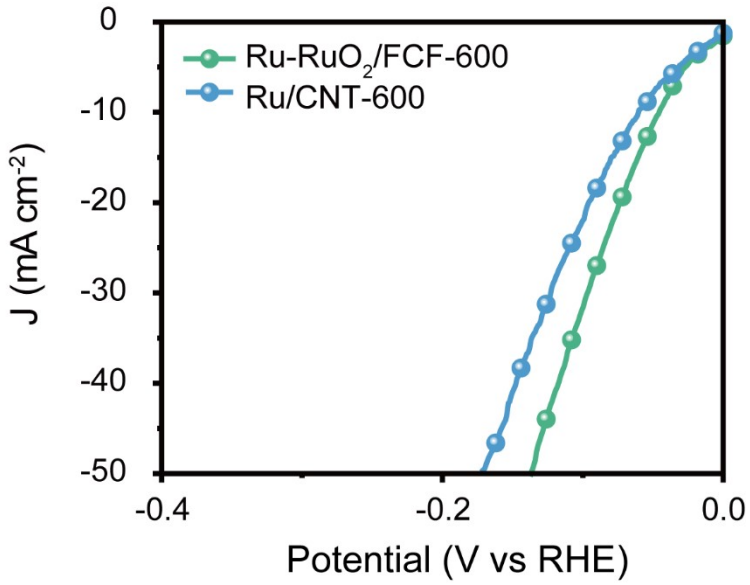

Figure S10. LSV curves of Ru-RuO_2/FCF-600 and Ru/CNT-600.

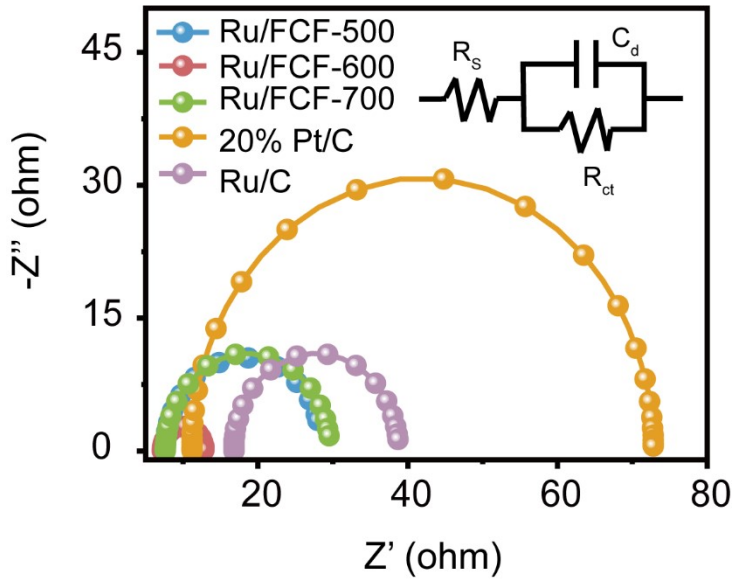

Figure S11. Nyquist plots of Ru/FCF-500, Ru/FCF-600, Ru/FCF-700, 20% Pt/C and commercial Ru/C of HER in 1.0 M KOH.

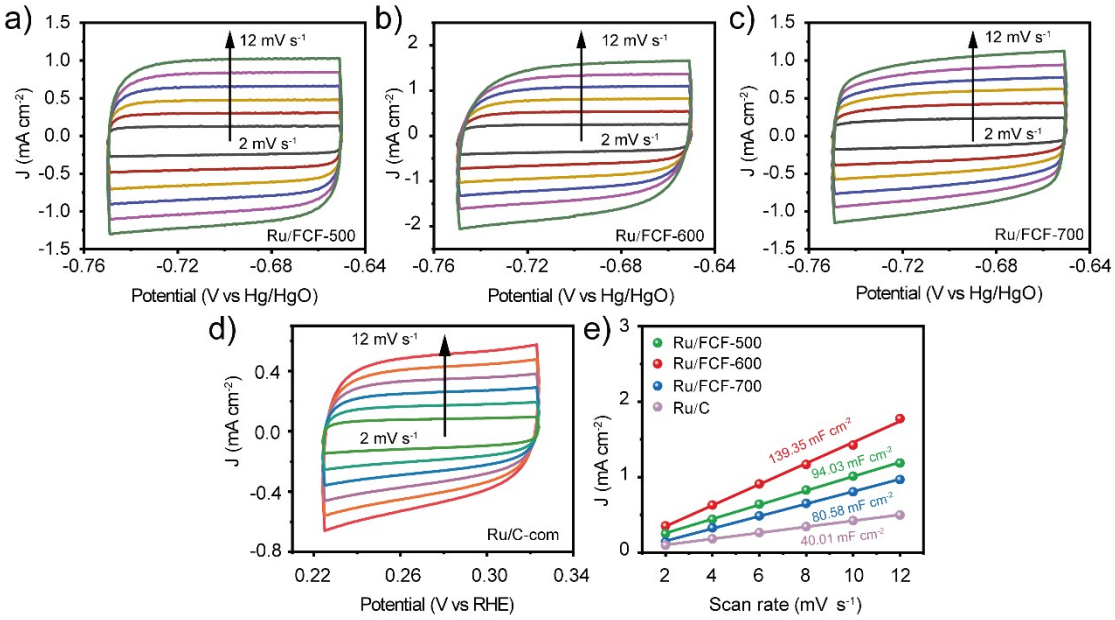

Figure S12. a) Ru/FCF-500, b) Ru/FCF-600, c) Ru/FCF-700 with a scan rate of 2, 4, 6, 8, 10, and 12 mV s^{-1} in 1 M KOH. d) The corresponding plots of current density difference against scan rate.

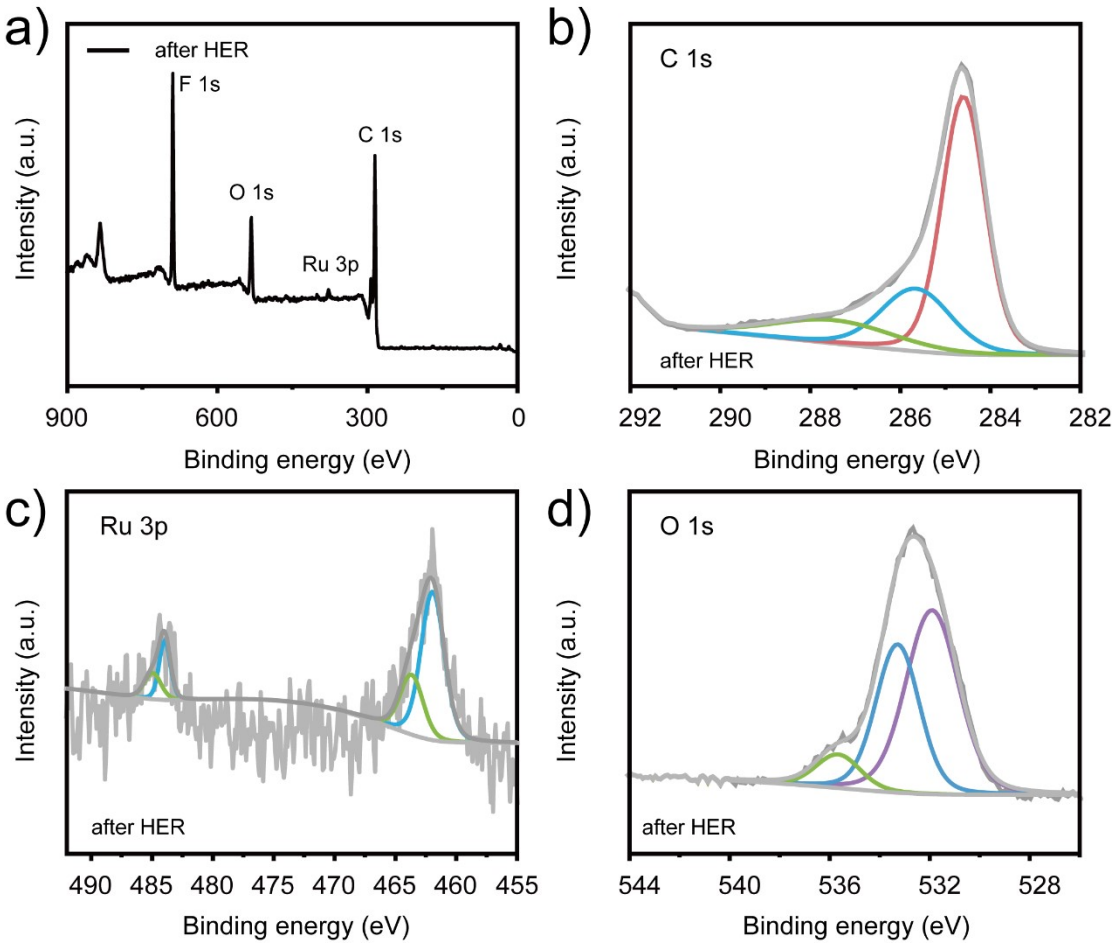

Figure S13. XPS spectra of Ru/FCF-600 after HER measurement. a) XPS survey spectrum, b) C 1s, c) Ru 3p, d) O 1s.

The fluorine (F) element signal detected in XPS survey spectrum S9a after the stability test is presumably attributed to the perfluorosulfonic acid polymer (Nafion binder) employed in the preparation of the working electrode, featuring a molecular structure rich in fluorine atoms.

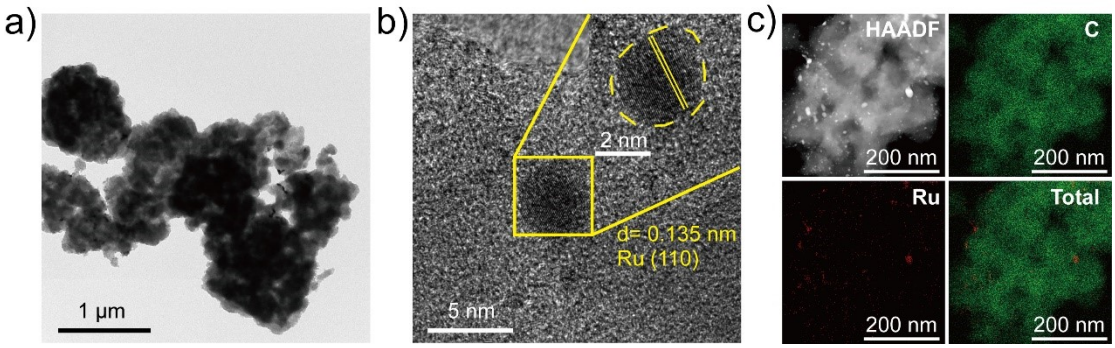

Figure S14. Structural and morphological characterization of Ru/FCF-600 after stability testing in 1 M KOH. a) TEM image, b) HRTEM image, c) SAED pattern, d) Corresponding elemental mapping images of C (green) and Ru (red).

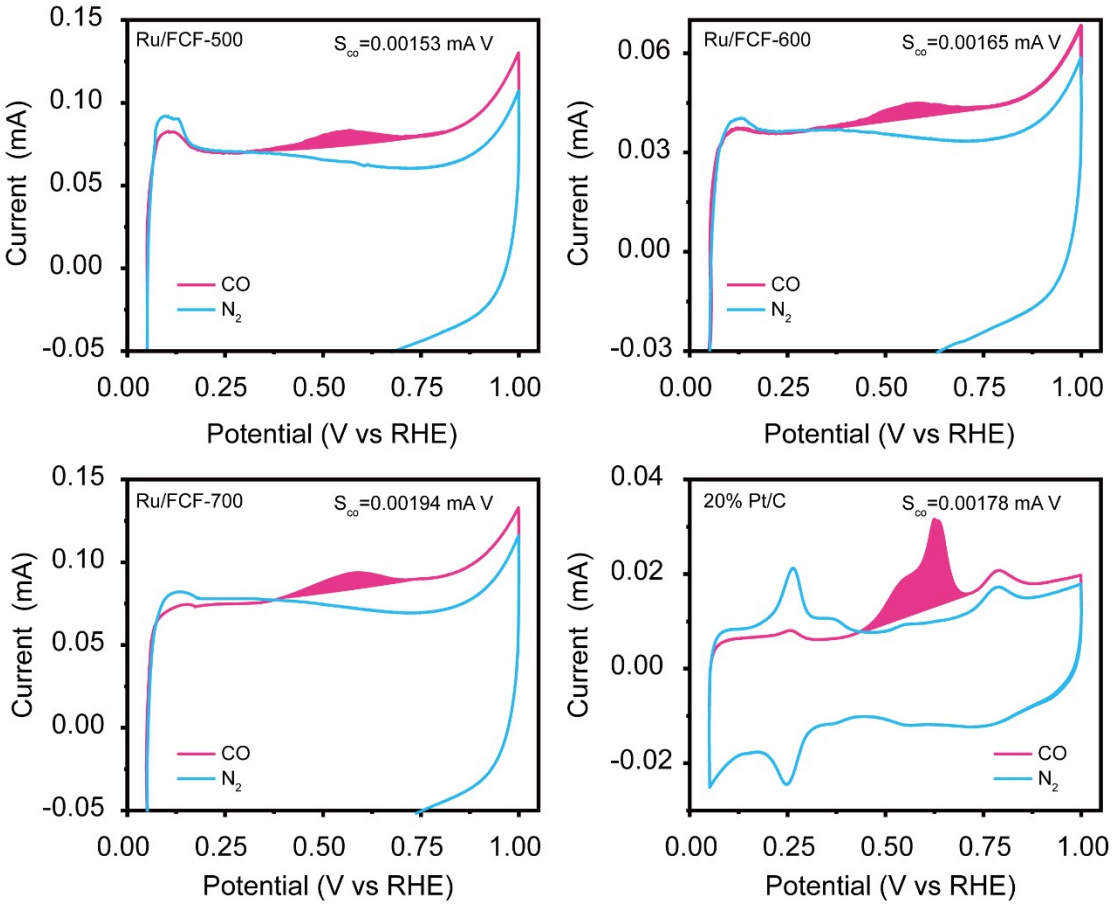

Figure S15. a-d) Background cycles (blue curves) and subsequent CO-stripping cycles (red curves) for Ru/FCF-500, Ru/FCF-600, Ru/FCF-700, and commercial Ru/C, respectively. The corresponding stripping charges, indicated by the red shaded areas, are obtained from the integrated peak areas.

Table S1. HER performance of the Ru/FCF-600 electrocatalyst in 1 M KOH.

Sample	η_{10} (mV)	Tafel slope (mV dec^{-1})	ECSA (cm^2)	R_{ct} (Ω)
Ru/FCF-500	58	137.60	94.03	21.02
Ru/FCF-600	23	37.80	139.35	5.59
Ru/FCF-700	62	70.70	80.58	21.96
20% Pt/C	57	85.60	--	61.65
Ru/C	77	73.72	40.01	22.02
Ru-RuO_2/FCF-600	46	--	--	--
Ru/CNT-600	61	--	--	--

Table S2. Comparison of TOFs of the Ru/FCF-600 under alkaline conditions with other reported HER catalysts.

No.	Catalyst	Overpotential (V)	TOF per active site (H_2 s^{-1})	Reference
1	Ru/FCF-600	0.10	21.42	This work
2	20% Pt/C	0.10	7.62	This work
3	Ru/C_{60}-300	0.10	10.50	Angew. Chem. Int. Ed. 2025, 64, e202414149
4	RuNi/CQDs	0.10	5.03	Angew. Chem. Int. Ed. 2020, 59, 1718.
5	Ru_{NPs}-$RuCr_{APs}$-N-C	0.10	13.15	Adv. Mater. 2025, 37, 2419360
6	Ru/Ni_3V-LDH	0.10	3.49	J. Am. Chem. Soc. 2021, 144, 1174.
7	$Ru@Mn_3O_4$	0.10	8.50	Angew. Chem. Int. Ed. 2025, e202504667
8	$Ru_{1,n}$-$ZnFe_2O_x$-C	0.05	10.30	Small. 2022, 18, 2204155.
9	Ru/O-CNT	0.05	2.96	Adv. Funct. Mater. 2025, 35, 2418617.
10	c-PRP DWNT/C	0.05	6.55	Adv. Energy Mater. 2024, 14, 2304269.
11	Ru/NDC-4	0.05	13.4	Appl. Catal., B **2023**, 327, 122466.
12	Ru_{SA+NC}/NiO-NF	0.05	1.91	Appl. Catal., B **2023**, 325, 122316.
13	RuP/C	0.02	3.50	Adv. Mater. 2018, 30, 1800047.
14	Ru/p-NC	0.025	8.90	J. Mater. Chem. A 2021, 9, 12196.
15	Ru-FeP-CoP/NPC	0.15	13.22	Ca rbon Energy. 2025, 7: e690.
16	$NiFeRu_{SA}$-DOBDC	0.20	18.20	Adv. Energy Mater. 2025, 15, 2404714.

Table S3. Summary of the recently reported Ru-based HER catalyst in 1 M KOH.

No.	Catalyst	η_{10} (mV)	reference
1	Ru-RuO_2/C_{60-x}	7	Angew. Chem. Int. Ed. 2025, e202503608.
2	Ru/FCF-600	23	This work
3	RuAu-0.2	24	Adv. Energy Mater., 2019, 9, 1803913.
4	Ru@WNO-C	24	Nano Energy 2021, 80, 105531.
5	RuNiS-C	25	Carbon 2020, 162, 172e180.
6	RuB_2	25	ACS Energy Lett. 2020, 5, 2909.
7	RuCo NSs	26	Adv. Energy Mater. 2020, 10, 2002860.
8	Ru/P-TiO_2	27	Angew. Chem. Int. Ed., 2022,134, e202212196
9	$Ru_{d=2.4\ Å}$	27	Adv. Mater. 2024, 36, 2310699
10	Sr_2RuO_4	28	Nat. Commun. 2022, 13, 7784.
11	Ru/C	28.6	Appl. Catal. B 2023, 323, 122145.
12	$PrRu_{0.5}Co_{1.5}$	29	Chem.-Eur. J.2023, 29, e202300205.
13	PdH_x@Ru	30	J. Am. Chem. Soc 2023, 145 5710–5717
14	Ru-$NiSe_2$	30	Chem.-Eur. J.2023, 29, e202300205.
15	Ru/Ni-MoS_2	32	Appl. Catal. B 2021, 298, 120557.
16	cRu-Ni_3N/NF	32	Energy Environ. Mater. 2023, 6, e12318.
17	Ru_1-NiCoP	32	Angew. Chem. Int. Ed. 2023, 62, e202308800.
18	MOC-Ru	33	Adv. Mater. 2023, 35, 2303331
19	Ru_{NP}-Ru_{SA}@CFN-800	33	Adv. Funct. Mater. 2023, 33, 2213058.
20	Ru/g-C_3N_4-2	34	J. Mater. Chem. A 2021, 9, 15019-15026.
21	MoO_x-Ru hcp	34	ACS Nano 2022, 16, 14885-14894.

22	RuCo-CAT/CC	38	Adv. Energy Mater. 2023, 13, 2204177.
23	VO-Ru/HfO_2	39	Nat. Commun. 2022, 13, 1270.
24	Ru/HfO_2	39	Nat. Comm. 2022, 13, 1270
25	a-Ru@Co-DHC	40	Chin. J. Catal.2022, 43, 110-115.
26	MSOR1	43	Adv. Funct. Mater. 2023, 33, 2210939
27	Br-Ru-RuO_2/MCC	44	J. Colloid Interface Sci. 2023, 646, 391-398.
28	(Ru-Co)O_x	44.1	Angew. Chem. Int. Ed. 2020, 59, 17219-17224.
29	Ru@Co/N-CNTs-2	48	ACS Sustainable Chem. Eng. 2020, 8, 24, 9136-9144.
30	Ru-MoP NWAs/CFP	49.9	Dalton Trans., 2022, 51, 3875–3883.
31	Ru_1CoP/CDs-1000	51	Angew. Chem. Int. Ed. 2021, 60, 7234-7244.
32	$Ru_{0.10}$@2H-MoS_2	51	Appl. Catal. B-Environ. 2021, 298, 120490.
33	Ru/Co_4N-CoF_2	53	Chem. Eng. J. 2021, 414, 128865.
34	Ru SAs–Ni_2P	57	Nano Energy 2021, 80, 105467.
35	Ru-$NiPS_3$	58	Nat. Commun. 2023, 14, 6462.

Table S4. Summary of the recently reported Ru-based OWS catalyst in 1 M KOH.

No.	Catalyst	E_{10} (mV)	reference
1	Ru@V-RuO_2/C HMS	1.437	Adv. Mater. 2023, 35, 2206351
2	RuO_2-300Ar	1.45	Energy Environ. Sci. 2021, 14, 5433
3	Ru-MoO_{3-x} NF || Fe_3O_4-NiFe LDH NF	1.46	Renewable Energy 2021, 177, 1346-1355.
4	Ru/FCF-600 || IrO_2	1.47	This work
5	Ru-NiFeP/NF	1.47	Appl. Surf. Sci. 2021,536, 147952.
6	Ru-MnFeP	1.47	Adv. Energy Mater. 2021, 10, 2000814.
7	CoRu/C	1.49	Chem. Eng. J. 2024, 492, 152337
8	M_2Ru_1 || M_2Ru_1O	1.49	Nano Res. 2022, 15, 1020-1026.
9	RuCo@CDs	1.50	J. Mater. Chem. A 2020, 8, 19, 9638-9645.
10	Ru/Co-N-C-800 ℃	1.50	Adv. Mater. 2022, 34, 2110103.
11	Ru/RuS_2-2	1.501	Angew. Chem. Int. Ed. 2021, 60, 12328.
12	NiFeRu-LDH	1.52	Adv. Mater. 2018, 30, 10, 1706279.
13	Pt/C/NF || RuO_2/NF	1.53	ChemCatChem 2022, 14, e202201010
14	20% Pt/C || IrO_2	1.54	This work
15	Ru/RuO_2-MoO_2(RRMC-500)	1.54	J. Colloid Interface Sci. 2021, 604, 508-516.
16	Ru_{NP}-Ru_{SA}@CFN-800 || IrO_2	1.54	Adv. Funct. Mater. 2023, 33, 2213058.
17	Ru/RuO_2/NC||RuO_2	1.58	Chem. Eng. J. 2022, 437, 135456.
18	RuNi nanoplates	1.58	Nano Energy 2018, 47, 1-7.
19	Ru-FeRu@C/NC||Ru-FeRu@C/NC	1.63	Chem. Eng. J. 2022, 437, 135456.
20	Ru@N-graphene	1.65	ACS Catal. 2019, 9, 11, 9897-9904.

Table S5. The comparison of AEMWE performance for Ru/FCF-600 with other reported electrocatalysts in alkaline solution.

Cathodic catalysts	Anodic catalysts	Activity	reference
Ru/FCF-600	IrO_2	1.65V@ 1A cm^{-2}	This work
NS-Ru	Commercial IrO_2	1.70V@ 1A cm^{-2}	Adv. Funct. Mater. 2023, 33, 2212321.
MoO_2@Ru	NiFe-LDH/NF	1.78V@ 1A cm^{-2}	Adv. Energy Mater. 2023, 13, 2301492.
MnRu/C_{60}-3	NiFeLDH	1.79V@ 1A cm^{-2}	Adv. Funct. Mater. 2024, 2409406.
Ru_1-Mo_2C	NiFe-LDH/NF	1.83V@ 1A cm^{-2}	Energy Environ. Sci. 2024, 17, 1397-1406.
Pt@S-NiFe LDH	S-NiFe LDH	1.90V@ 1A cm^{-2}	Adv. Mater. 2023, 35, 2208209.
20% Pt/C	IrO_2	1.91@ 1A cm^{-2}	This work
CeO_2-Ru aerogel	NiFe-LDH/NF	1.99V@ 1A cm^{-2}	Adv. Energy Mater. 2025, 15, 2405681.